

Subject-specific blood flow simulation in the human carotid artery bifurcation

M. D. Deshpande^{1,*}, Vinay Ballal¹, S. R. Shankapal¹, Vinay M. D. Prabhu² and M. G. Srinath²

¹M.S. Ramaiah School of Advanced Studies, Bangalore 560 054, India

²M.S. Ramaiah Medical College and Hospitals, Bangalore 560 054, India

Pulsatile blood flow in the human carotid artery bifurcation has been simulated by solving the incompressible Navier–Stokes equations. Subject-specific data were obtained from two volunteers. Three-dimensional vascular geometry was extracted from magnetic resonance imaging scans and periodic velocity profiles were constructed using Doppler ultrasonography and used as boundary conditions. Flow separation and associated reversed wall shear stress were observed in some bifurcations. Even mild stenoses that do not affect the overall blood flow were associated with a significant local flow alteration.

Keywords: Atherosclerosis, computational fluid dynamics, Doppler ultrasound, flow separation, magnetic resonance imaging.

AN estimated 17.5 million people died due to cardiovascular disease worldwide in 2005, representing 30% of the deaths. About 80% of these deaths took place in the low- and middle-income countries. If current trends are allowed to continue, by 2015, an estimated 20 million people will die from cardiovascular disease, mainly from heart attacks and strokes^{1,2}.

Observations have shown that there is a correlation between certain forms of blood flow like separated flows and wall alterations^{3–6}. Such phenomena take place in vessel bifurcations or bends and are associated with sites prone to atherosclerosis. Presence of a vessel constriction or stenosis further distorts flow. Wall shear stress (WSS) is generally high in the stenotic region and a high velocity jet issuing from here continues for some distance. Flow may separate in this region resulting in reversed WSS. Due to the low and moderate values of the Reynolds number, the flow may become disturbed and highly chaotic in certain parts in the presence of a stenosis, but it does not necessarily mean it has become fully turbulent as verified from the direct numerical calculations by Lee *et al.*⁷.

The flow field in the presence of a stenosis in a straight or branching tube has been of interest due to its associa-

tion with atherosclerosis even though precise relations between the two are not known. However, it is hoped that a subject-specific flow simulation may help in diagnosis, surgical planning and risk assessment. A reliable flow simulation requires an accurate definition of vascular geometry, which is necessarily three-dimensional and velocity boundary conditions which are unsteady. Two magnetic resonance (MR) images of the neck area from a volunteer (subject B in this study) shown in Figure 1 indicate the complexity of the geometry involved. The carotid bifurcation comprises the common carotid artery (CCA), the carotid bulb and bifurcation into the internal and external carotid arteries (ICA and ECA). Developments in computational fluid dynamics (CFD), flow visualization techniques and capabilities in medical image processing are helpful in such flow simulations. The human carotid bifurcation has been chosen for the current study as its geometric definition can be obtained using ultrasonography (US), computed tomography (CT) or magnetic resonance imaging (MRI) techniques. Pulsed Doppler US can be used to obtain velocity boundary conditions since the carotid bifurcation is easily accessible being close to the skin.

Over the last four decades, several efforts have been made with simulations, *in vitro* laser Doppler anemometer (LDA) measurements and flow visualizations to understand stenotic and branching vascular flows. Deshpande *et al.*⁸ made flow simulations in case of localized axisymmetric stenosis. Deshpande and Giddens⁹ reported detailed turbulent flow fields using LDA. A critical review of the stenotic flow is available in Berger and Jou¹⁰. Flow measurements have been made with carotid arterial models for steady flow by Bharadvaj *et al.*¹¹ and for unsteady flows by Ku and Giddens¹². Flow simulations have been made in rigid bifurcation models by Jou and Berger¹³, assuming compliant wall by Perktold and Rappitsch¹⁴ and also assuming blood to be a non-Newtonian fluid by Gijzen *et al.*¹⁵. Subsequently, several studies^{7,16–18} have been undertaken obtaining geometric and flow velocity data from human subjects using MRI, phase contrast magnetic resonance angiography (MRA) and pulsed Doppler US.

In the present study, a systematic approach was adopted wherein the computations have been made for modelled geometries and compared with both steady and unsteady

*For correspondence. (e-mail: deshpande@msrsas.org)

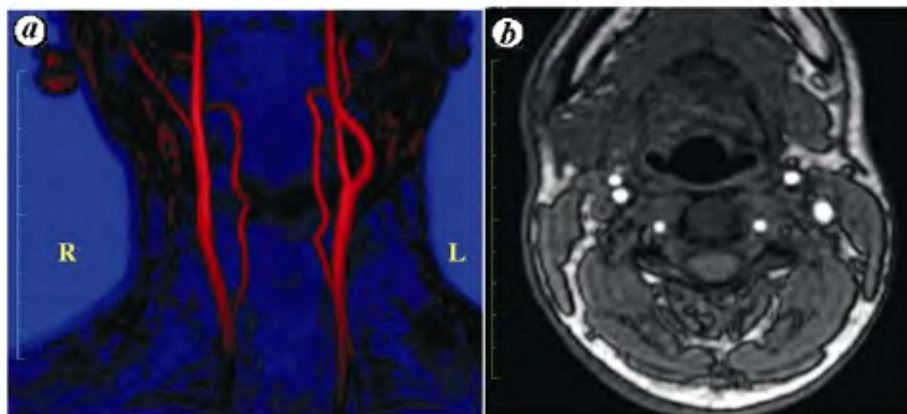


Figure 1. MR images of the neck and adjoining region for subject B. Smallest unit on the scales shown is 1 cm. *a*, Volume rendered three-dimensional time-of-flight MRA of the carotid and vertebral arteries viewed from the front; *b*, Axial cross-section through the neck viewed from below.

experimental data. After establishing the reliability of the CFD procedure, it was applied to three human carotid bifurcation geometries from MRI of two volunteers using three-dimensional Time-of-Flight Angiography (Signa HDx 1.5T, GE Healthcare). The three-dimensional geometries extracted from the MRI were further improved in their geometrical accuracy using US. Velocity boundary conditions were constructed from pulsed Doppler US data obtained at seven radial locations of the inlet plane of the CCA and from the exit planes of the ICA and ECA (Voluson, 730 PRO, GE Healthcare). The measurements from two male human volunteers aged 63 years (subject A) and 24 years (subject B) were made non-invasively using MRI and Doppler US. An informed consent was obtained before their participation. This study received approval of the Ethical Review Board of M.S. Ramaiah Medical College and Teaching Hospital, Bangalore.

Preliminary computations

Several exercises were carried out initially to establish a procedure, validate the reliability of the commercial software tools used and to establish the reliability of the simulated results by comparing them with experimental data available in the literature. For this reason, the models used in this section are those for which LDA data are available. Extensive testing and grid independence study were carried out regarding flow simulation, some of which are described here.

The geometry shown in Figure 2 was created from the dimensions specified by Bharadvaj *et al.*¹¹ using CATIA version P3 V5R17 software for geometric modelling and Gambit version 2.2.30 software for grid generation. The unstructured grid shown has 1,309,000 cells, 90% of which are hexahedral, the remaining being tetrahedral and pyramidal. The cross-sections of the CCA, ICA (left branch in Figure 2) and the ECA (right branch in Figure 2) were circular in this model but special care was needed at

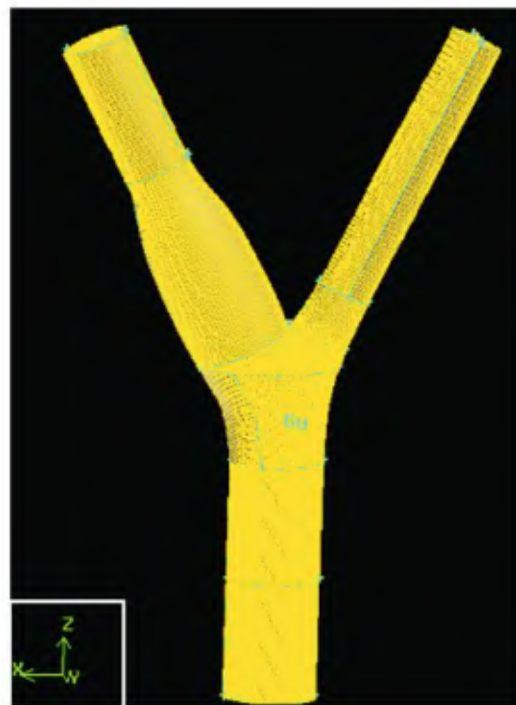


Figure 2. Geometry and grid for the carotid artery model from Bharadvaj *et al.*¹¹.

the bifurcation region while generating surface geometry and grid.

Incompressible flow solution was obtained by solving the continuity and the Navier–Stokes equations using FLUENT version 6.3.26 software. Calculations were done for several values of Reynolds number $Re = UD/\nu$, where U is the average flow velocity at the entrance plane of the CCA of diameter D and ν the kinematic viscosity of the fluid. The inlet velocity profile was parabolic and steady to match the experimental value of Bharadvaj *et al.*¹¹. The exit boundary conditions were applied with a specified division of flow between the ICA and ECA

branches. The no-slip boundary condition was specified on the wall. Since the flow was steady it was solved iteratively for a given value of Re .

The streamline patterns are shown in Figure 3 for $Re = 400$. Here, the flow division between the ICA and ECA was 70% and 30%, respectively, the value selected to match the experimental case¹¹. A separation region is clearly seen in the sinus of the ICA along its outer wall. Length of the separation eddy is seen to increase with Re . A comparison with the experimental data¹¹ for the axial velocity distribution along the centrelines of the CCA and the ICA is satisfactory as shown in Figure 4.

Comparison with unsteady data

Measurements in unsteady flow using LDA are reported by Ku and Giddens¹². The same model as that used in the

steady flow study¹¹ was used here. A periodic inlet velocity boundary condition was used in the experiments to mimic a pulsatile human cardiac output. We used this inlet boundary condition measured from a graph. The non-dimensional parameter describing the unsteady flow is the Womersley number $W = R\sqrt{\omega/\nu}$, based on $R = D/2 =$ radius of the CCA and radial frequency ω of the periodic flow. A value of $W = 4.0$ was selected to match the experiments. A good agreement is seen with the experimental WSS time trace in Figure 5. The velocity profile at a particular location in the ICA at a particular instant identified by the phase angle of 75° is compared with the experimental data in Figure 6. And the comparison is satisfactory.

These preliminary exercises involved a fairly complicated geometry, especially near the apex of the bifurcation. Special attention was required when applying boundary conditions for a specified division of flow

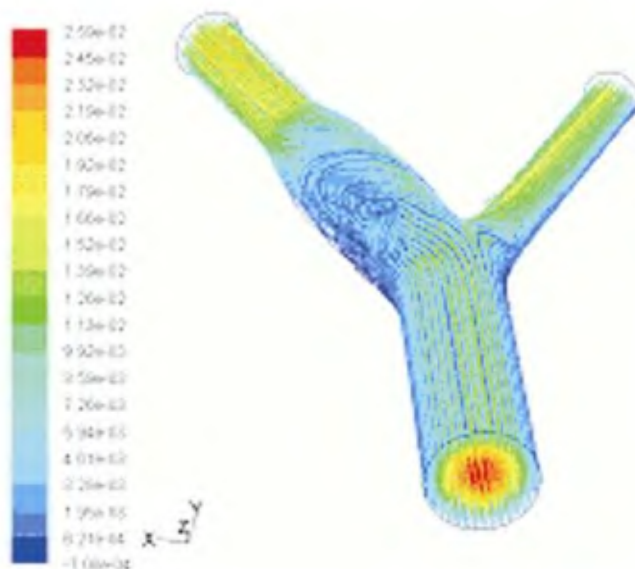


Figure 3. Streamlines simulated in the model of Bharadvaj *et al.*¹¹ and coloured by Z-velocity. Steady flow. $Re = 400$.

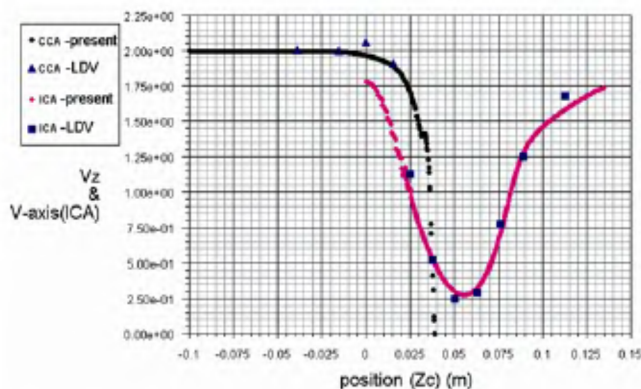


Figure 4. Comparison of centreline axial velocity with the experimental LDV data of Bharadvaj *et al.*¹¹ in the CCA and ICA of the modelled carotid bifurcation. $Re = 400$.

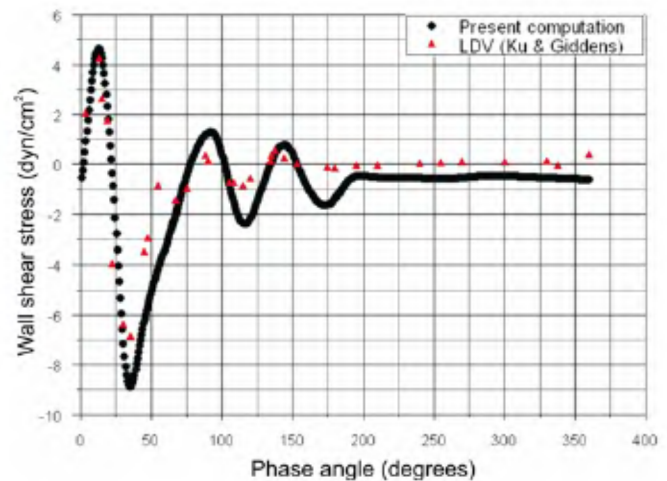


Figure 5. Wall shear stress as a function of phase angle in the CCA compared with experimental data of Ku and Giddens¹². Peak $Re = 800$, $W = 4.0$ and $Xc = 0.9 D$.

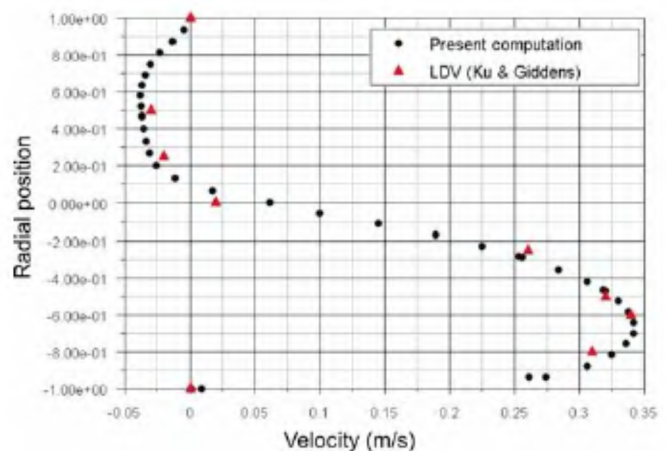


Figure 6. Axial velocity profiles in the proximal ICA at the axial location $0.9 D$ in the plane of bifurcation (phase angle = 75°). Comparison with experimental data of Ku and Giddens¹². Peak $Re = 800$, $W = 4.0$.

between the daughter branches. Acquiring and processing subject-specific data pertaining to the human carotid bifurcation required special effort, as described in the next section.

Subject-specific flow simulations

A reliable subject-specific blood flow simulation requires an accurate measurement of the arterial geometry and also velocity profiles at the inlet and exits. Despite the developments in modern radiological equipment, these two aspects remain the major source of uncertainty and deserve special attention. Further, in this study the geometry is assumed to be rigid and blood, a Newtonian fluid. These two approximations are less serious in nature and also making them subject-specific is not easy. Our efforts have been aimed at minimizing the two major sources of error.

Extracting vascular geometry and grid generation

From the MRI of subject B shown in Figure 1, the three-dimensional geometry of the carotid artery for the right and left sides was extracted separately using MIMICS 8.11 software. The right carotid bifurcation of subject B (named BR) is shown in Figure 7 *a*. Subsequently, it was modified for its dimensional accuracy using US image data and the surface was created using CATIA software. The computational domain is shown in Figure 7 *b* and it

has 402,976 grid cells. The computational domain is shorter than the original geometry extracted from MRI. Several factors play a role in this selection. Ideally one would like to have the computational domain to extend as far as practicable from the region of the bifurcation which is of interest. Extending the region too far leads to inclusion of secondary branches in the ECA which is undesirable in the present context. Extended computational domain also means a longer computational time. But the deciding factor in this study was the limitation of the pulsed Doppler US in making accurate measurements beyond a certain distance from the bifurcation on either side due to the artery being inaccessible deeper inside the body. However, the lengths we have chosen are at least comparable to those in the Wake's study¹⁸ where a phase contrast MRA was used for velocity measurements. Also, because of the same difficulty, satisfactory measurements could not be obtained in the left carotid bifurcation of subject A (i.e. case AL) hence this was excluded from the study. However, there was no difficulty with the right carotid bifurcation of subject A (case AR) which was included in this study along with the right carotid bifurcation (case BR) and left carotid bifurcation (case BL) of subject B.

Boundary conditions

The accuracy of the flow simulation depends to a great extent on the ability to apply boundary conditions accurately. Velocity profiles in the inlet plane are needed as a function of time. Usually one of the two extreme cases is chosen where the profiles are either flat or parabolic¹⁹. An improved approach is to assume that the flow is periodic and fully developed and hence use the Womersley profiles⁷. However, it is likely that the actual profiles will be far from these idealized cases. There have also been efforts using phase contrast MRA to obtain velocity boundary conditions for the entire cross-section¹⁸. With the available pulsed Doppler US technique, an improved method has been attempted in the present study. The blood velocity was measured at seven radial points located symmetrically. Time trace at one such radial location is shown in Figure 8 along with the calliper location on the beam. The calliper width was kept at the minimum value possible (specified by the manufacturer to be 0.7 mm). Note that the beam is inclined 60° to the axis of the CCA. From a single cardiac cycle in this figure, the maximum values of the velocity were read out at 51 instants spaced uniformly. Observations from the measurements at seven radial locations showed that the profiles were nearly symmetrical along the diameter chosen. Assuming axisymmetry and no-slip at the arterial wall, a cubic profile was fitted with the least square technique at each instant. The velocity profiles obtained in this fashion are shown in Figure 9 for case BR. It may be noted that

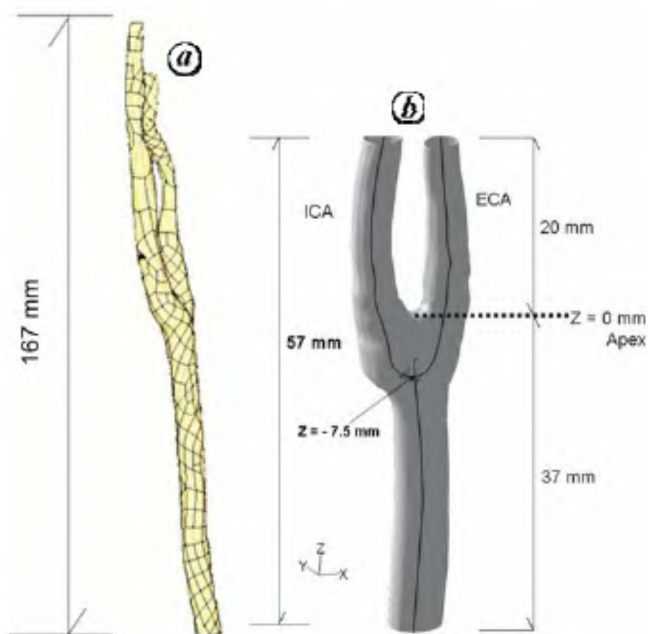


Figure 7. Right carotid arteries of subject B. (*a*) Geometry extracted from MRI using MIMICS software. Diameter of the CCA is 6.0 mm. (*b*) Surface modelling and computational domain used for CFD calculations.

they are not close to uniform or parabolic but somewhat similar to the Womersley profiles.

A similar procedure was applied at the exit planes of the daughter arteries. Since the measurement procedure at seven locations and in three planes took about 60 min, a flow rate balance is required so that the sum of outflows is equal to the flow at the inlet. The measurements at the daughter artery exits are likely to be less accurate due to their smaller diameter and also because the flow is likely to be non-axisymmetric. The corrected flow rates obtained in this fashion are shown in Figure 10 and the percentage division between them in Figure 11. Thus, it amounts to using the velocity profiles at the exit planes with regard to their contribution to flow rate but not their detailed shapes.

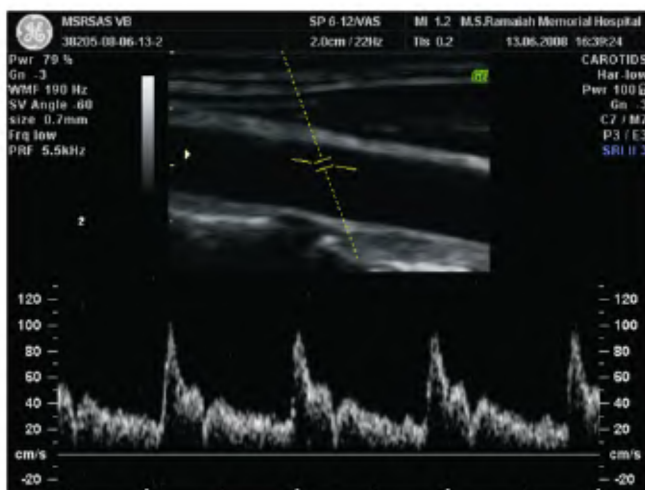


Figure 8. Pulsed Doppler ultrasound measurements at a localized radial position in the right CCA of subject B. Beam and calliper locations are indicated. Flow is from right to left. Seven such measurements were used to construct velocity profiles as the velocity boundary condition.

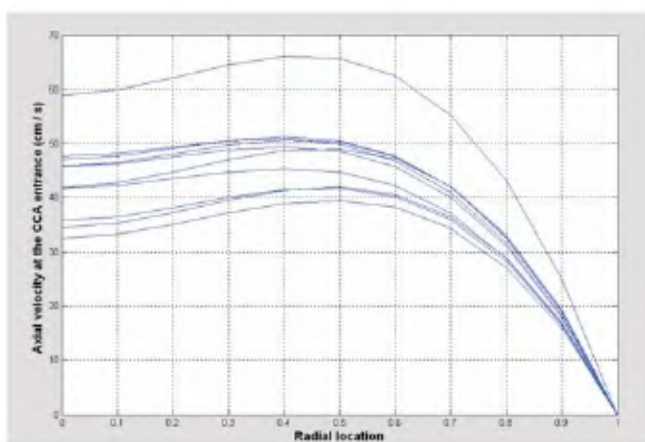


Figure 9. Axial velocity profiles for case BR at the inlet section of CCA for 10 equally spaced times in the cardiac cycle. These were constructed from the pulsed Doppler ultrasound signals taken at seven radial locations in the CCA. Peak $Re = 1725$, $W = 4.59$.

Results and discussion

Numerical flow simulations have been carried out for the three cases AR, BR and BL for the measured values of Re and W and the flow division between the two branches. Blood viscosity was estimated from the haematocrit measurement from blood samples in each case⁵. Computations were also carried out with extended parameters like varying Re and W in case BR. Additionally computations were done for three grades of stenoses simulated in the ICA of case AR. It was found adequate to calculate the flow for two cycles to establish periodicity. Computations typically took about 130–160 h for each case on the XW8200 HP Work Station.

Instantaneous streamline patterns are shown in Figure 12 at four different instants for case BR for peak $Re = 1725$ and $W = 4.59$. Flow separation is seen mainly in the carotid bulb. Flow accelerates in both the branches along the axis but the velocity in the ICA is generally higher, except at peak systole where the velocity in the ECA is comparable to that in the ICA. In-plane velocity vectors at four different times in a cycle at $Z = -0.5$ mm representing a plane in the bifurcation are shown in Figure 13 for case BR and are coloured by the axial velocity magnitude. A clockwise spiral in the ICA and counter-

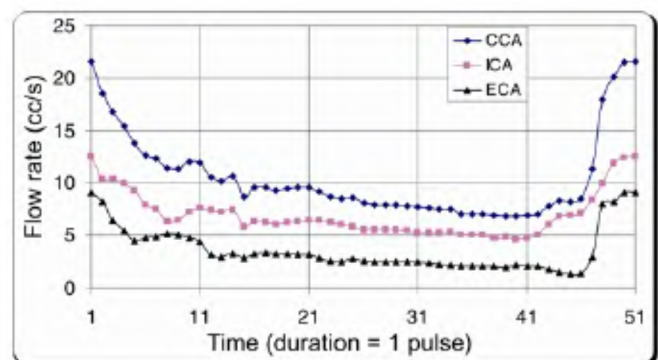


Figure 10. Velocity boundary conditions during one cycle of the heart beat of subject BR (discretized into 50 divisions) after mass conservation corrections were applied. Peak $Re = 1725$, $W = 4.59$.

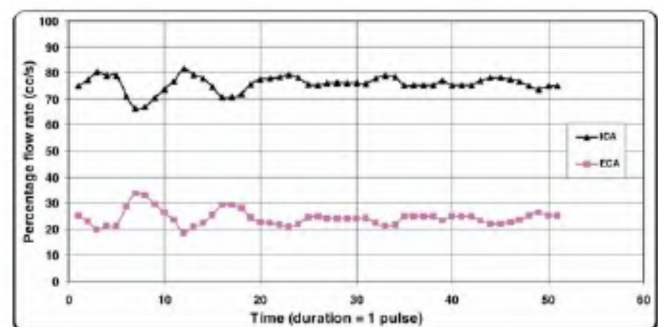


Figure 11. The flow division between the ICA and ECA during one cycle is calculated from the previous figure and is used as the boundary condition at the exit planes of the ICA and ECA.

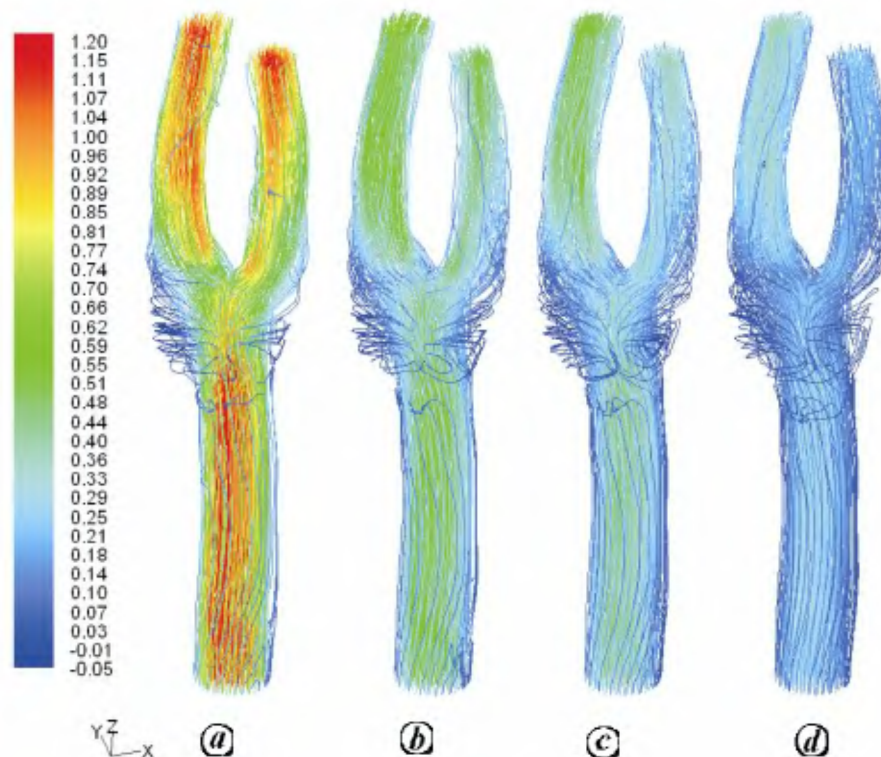


Figure 12. Instantaneous streamline patterns in the carotid bifurcation in case BR at non-dimensional time $T = 0, 0.1995, 0.3992$ and 0.7983 . Peak $Re = 1725$, $W = 4.59$. Flow separation is present in the ICA at all times but intermittent in the ECA.

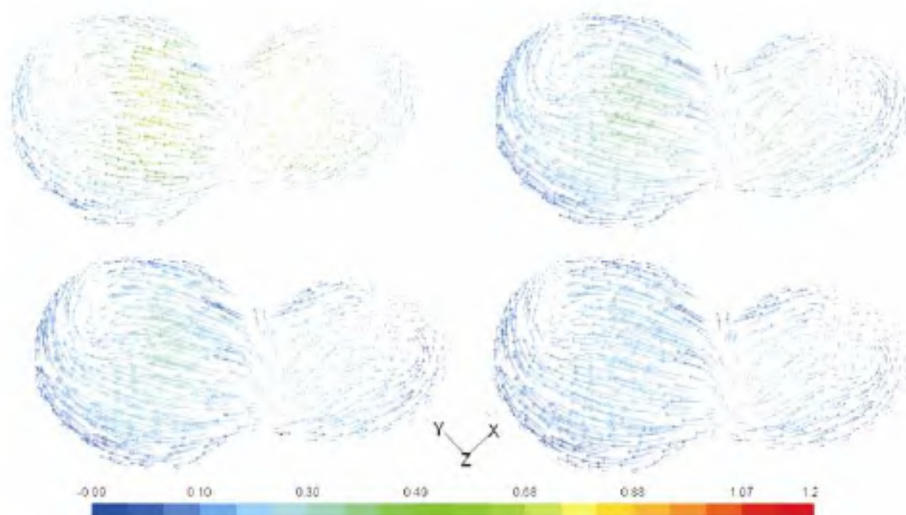


Figure 13. Velocity vectors at four different times at $Z = -0.5$ mm in the carotid bulb in case BR. Peak $Re = 1725$, $W = 4.59$.

clockwise spiral in the ECA indicate helical streamlines winding in opposite directions. The streamline patterns are consistent with the WSS contours in Figure 14. A negative value is seen in a large area in the carotid bulb where it is also oscillatory, a factor suspected to be associated with atherosclerosis^{3,5}. It is of interest to note that the left carotid bifurcation of the same subject (case BL)

does not show any flow separation possibly due to a straight geometry as seen in Figure 15.

Streamline pattern for case AR shown in Figure 16 indicates a separated flow mainly in the ICA. In this case, the branches are tortuous or wavy in morphology as the sample is from an older individual. Contours of Z-velocity at various cross-sections as shown in Figure 17a indicate

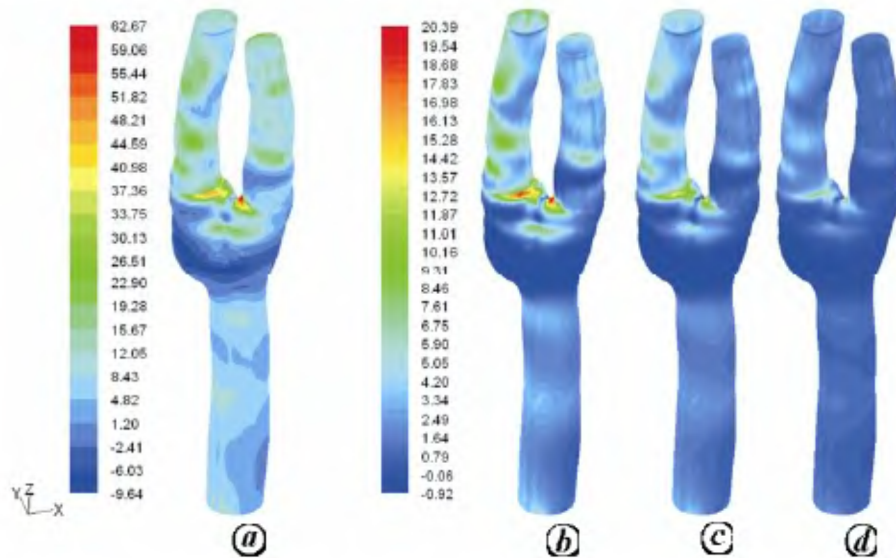


Figure 14. Contours of wall shear stress in the carotid bifurcation in case BR at non-dimensional time $T = 0, 0.1995, 0.3992$ and 0.7983 . Peak $Re = 1725$, $W = 4.59$. Extent of flow separation can be seen in both the ICA and ECA by negative shear stress. Highest wall shear stress occurs near the apex of the branch. Wall shear stress is higher in the ICA as compared to the ECA.

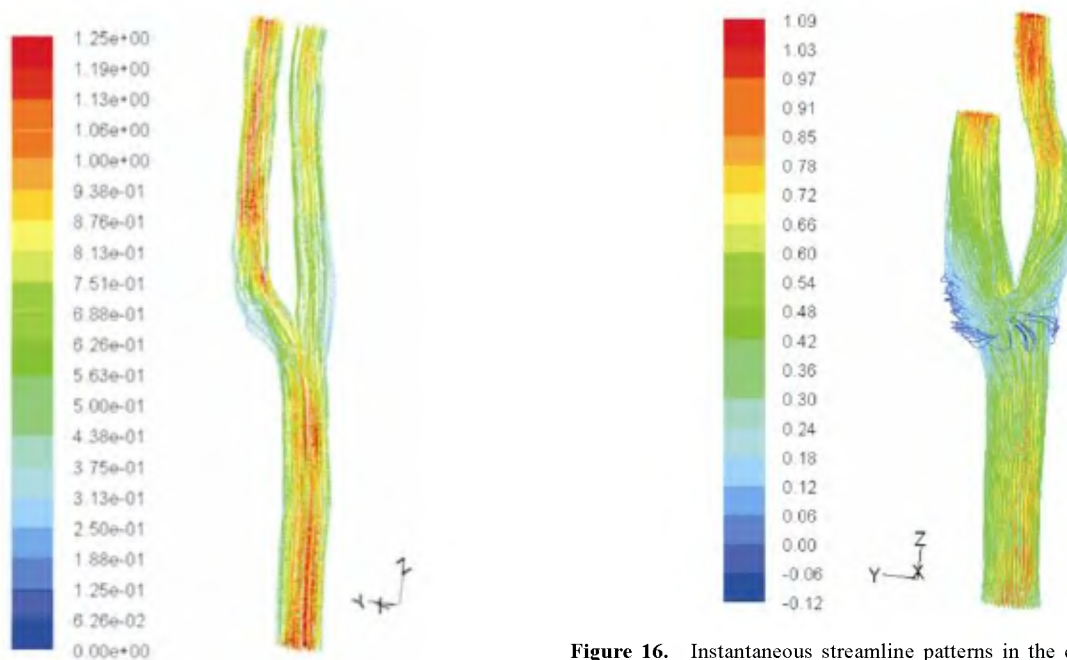


Figure 15. Instantaneous streamline patterns in the carotid bifurcation in case BL (same subject as in the previous figure but the opposite side) at non-dimensional time $T = 0$, indicating peak systole. Peak $Re = 1765$, $W = 4.60$. Flow separation is not seen unlike in the opposite side (case BR).

Figure 16. Instantaneous streamline patterns in the carotid artery in the older subject AR at non-dimensional time $T = 0$. Peak $Re = 1266$ and $W = 4.07$. Flow is separated but mainly in the ICA. Flow velocity is higher at the ECA exit due to its smaller diameter.

Stenotic flows

the extent of flow reversal in the carotid bulb. Flow is nearly axisymmetric in the CCA but it has not quite reached such a state at the ICA and ECA exit planes. The maximum velocity in the ECA is about 1.1 m/s, somewhat higher due to its smaller diameter and it has also led to a higher WSS as shown in Figure 17 *b*.

To study the effect of stenosis on flow, using the geometry of case AR we have created a family of stenotic geometries ARS1, ARS2 and ARS3 with 50%, 85% and 95% area reduction respectively. The location and shape of isolated atherosclerotic plaques are somewhat unpredictable but the entrance of the ICA is one preferred location. Hence, the choice of this site. The choice of velocity

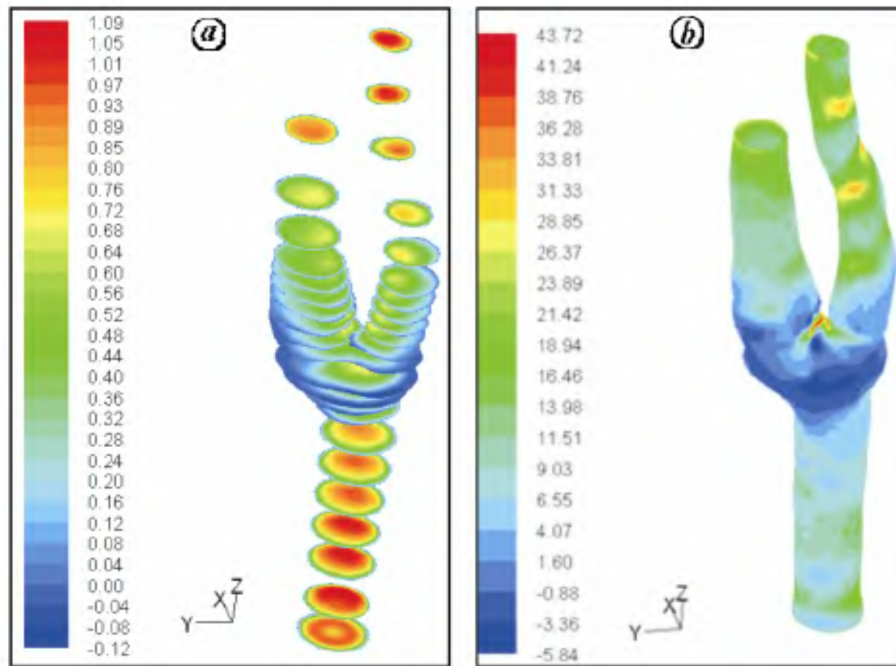


Figure 17. Contours in the carotid bifurcation in case AR at non-dimensional time $T = 0$. Peak $Re = 1266$ and $W = 4.07$. *a*, Contours of Z-velocity at various cross-sections; *b*, Contours of wall shear stress. Wall shear stress is higher in the ECA than in the ICA.

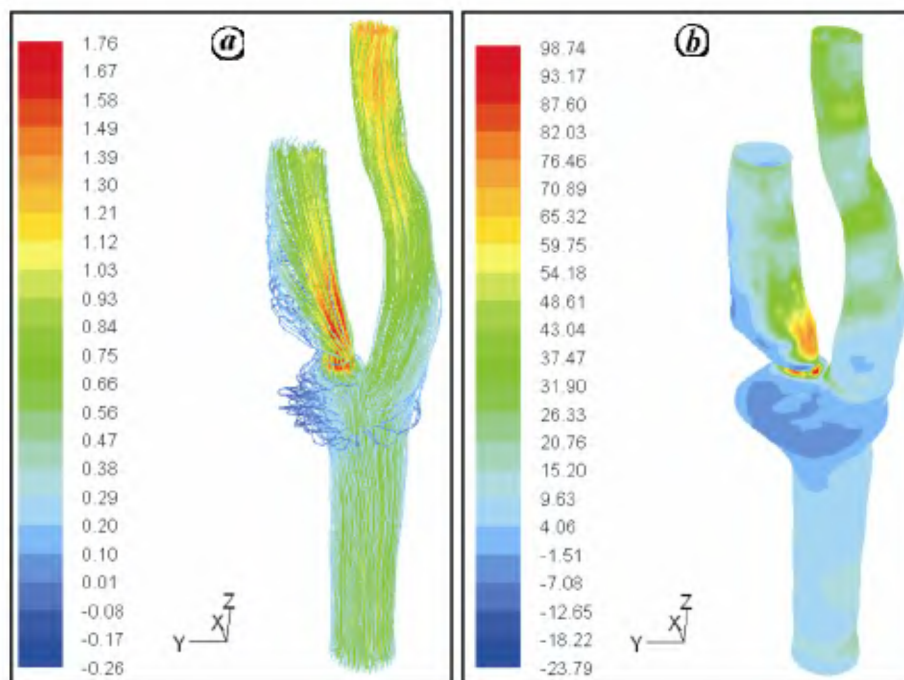


Figure 18. Stenosis Model ARS1 with 50% area reduction of ICA in subject A at non-dimensional time $T = 0$. Peak $Re = 1266$ and $W = 4.07$. *a*, Instantaneous streamline patterns depict flow separation proximal to the stenosis also; *b*, Contours of wall shear stress patterns indicate an increase in the magnitude of both positive and negative values.

boundary conditions is difficult especially when the degree of stenosis is severe. It is widely known that if area reduction is less than 70% the flow sharing between the ICA and ECA does not change significantly^{19,20}.

However, the local flow patterns get altered considerably as described here.

A streamline pattern for case ARS1 with a 50% area reduction as shown in Figure 18*a* exhibits an extension

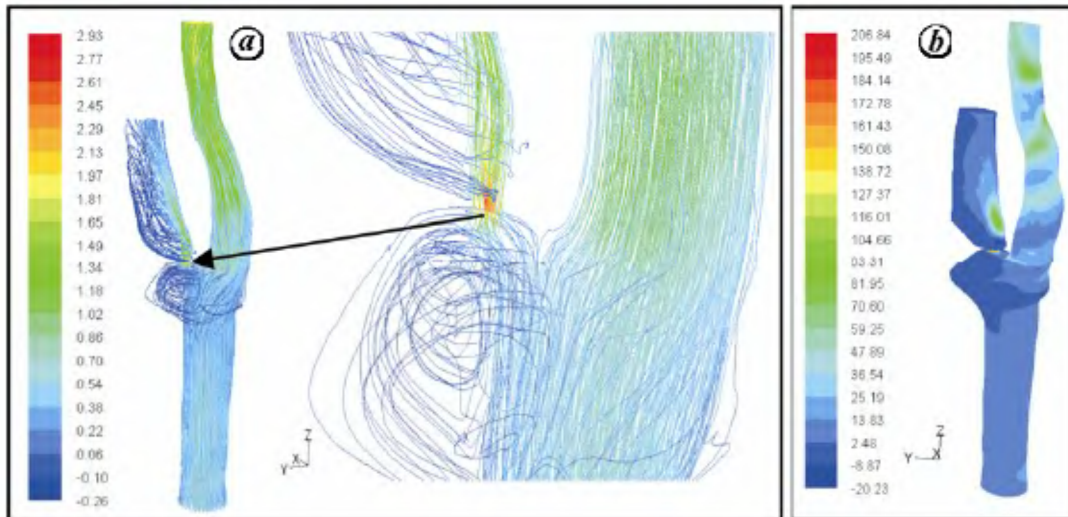


Figure 19. Stenosis Model ARS2 with 85% area reduction of ICA in subject A at non-dimensional time $T = 0$. Peak $Re = 1266$ and $W = 4.07$. **a**, Instantaneous streamline patterns depict massive flow separation proximal to the stenosis; **b**, Contours of wall shear stress.

in length of the separated region involving helical streamlines. The highest velocity observed is about 1.7 m/s, a substantial increase from the normal as in case AR shown in Figure 16. A considerable increase is also seen in WSS from its contours in Figure 18 *b*. Thus, even with only a 50% area reduction and no change in the flow rate, the local velocity and WSS increase significantly. A more drastic increase in velocity and WSS for case ARS2 with 85% area reduction is seen in Figure 19. The increased velocity in the post-stenotic region is of diagnostic value and various indices and methodologies assessing haemodynamically significant stenoses have been reported^{19,21–23}.

It may be noted that there was no indication of atherosclerotic plaques in the three carotid bifurcations AR, BR and BL from the two volunteers as observed under US and MR imaging. It was convenient to simulate stenotic geometries which allow parametric studies, as compared to obtaining such geometries from volunteers having such plaques.

Flow transition

Despite the complicated geometry of the carotid bifurcation, the flow generally remains laminar due to moderate values of $Re^{24,25}$. The presence of a stenosis makes the flow chaotic in the ICA for a limited interval of time during the decelerating phase of systole but the flow remains laminar in CCA and ECA as inferred by Lee *et al.*⁷ by direct numerical simulation. However, such simulations require a very long computational time. The present approach with a fine grid but with laminar viscosity may be adequate keeping in mind two major uncertainties, one is the need for a good definition of geometry and the

other, velocity boundary conditions. Using Reynolds-averaged Navier–Stokes equations and a turbulence model is not recommended as the flow is not actually turbulent.

Conclusion

Blood flow in the carotid bifurcation is associated with high WSS and also possible flow separation. The flow may be highly subject-specific and variations may be present even between the left and right sides. The presence of even what is considered a mild stenosis may alter the local flow considerably. Subject-specific flow quantification which may be of value in diagnosis, surgical planning and risk assessment requires an accurate determination of geometry and velocity boundary conditions. MRI and pulsed Doppler ultrasound combined with CFD techniques are useful in that direction. Details of flow that are available by this combined approach are far superior to those that may be obtained by medical imaging techniques alone.

1. World Health Report, WHO, 2006.
2. World Health Report, WHO, 2008.
3. Caro, C. G., Fitz-Gerald, J. M. and Schroter, R. C., Arterial wall shear stress and distribution of early atheroma in man. *Nature*, 1969, **223**, 1159–1161.
4. Ku, D. N., Giddens, D. P., Zarins, C. K. and Glagov, S., Pulsatile flow and atherosclerosis in human carotid bifurcation: positive correlation between plaque location and low oscillating shear stress. *Arteriosclerosis*, 1985, **5**, 293–302.
5. Fung, Y. C., *Biomechanics: Circulation*, Springer, New York, 1997, 2nd edn.
6. Lusis, A. J., Atherosclerosis. *Nature*, 2000, **407**, 233–241.

RESEARCH ARTICLES

7. Lee, S. E., Lee, S., Fischer, P. F., Bassiouny, H. S. and Loth, F., Direct numerical simulation of flow in a stenosed carotid bifurcation. *J. Biomech.*, 2008, **41**, 2551–2561.
8. Deshpande, M. D., Giddens, D. P. and Mabon, R. F., Steady laminar flow through modeled vascular stenoses. *J. Biomech.*, 1976, **20**, 407–421.
9. Deshpande, M. D. and Giddens, D. P., Turbulence measurements in a constricted tube. *J. Fluid Mech.*, 1980, **97**, 65–89.
10. Berger, S. A. and Jou, L.-D., Flows in stenotic vessels. *Annu. Rev. Fluid Mech.*, 2000, **32**, 347–382.
11. Bharadvaj, B. K., Mabon, R. F. and Giddens, D. P., Steady flow in a model of the human carotid bifurcation. Part II – Laser Doppler anemometer measurements. *J. Biomech.*, 1982, **15**, 363–378.
12. Ku, D. N. and Giddens, D. P., Laser Doppler anemometer measurements of pulsatile flow in a model carotid bifurcation. *J. Biomech.*, 1987, **20**, 407–421.
13. Jou, L.-D. and Berger, S. A., Numerical simulation of flow in the carotid bifurcation. *Theor. Comp. Fluid Dynam.*, 1998, **10**, 239–248.
14. Perktold, K. and Rappitsch, G., Computer simulation of local blood flow and vessel mechanics in a compliant carotid artery bifurcation model. *J. Biomech.*, 1995, **28**, 845–856.
15. Gijsen, F. J. H., van de Vosse, F. N. and Janssen, J. D., The influence of the non-Newtonian properties of blood on the flow in large arteries: steady flow in a carotid bifurcation model. *J. Biomech.*, 1999, **32**, 601–608.
16. Zhao, S. Z., Xu, X. Y., Hughes, A. D., Thom, S. A., Stanton, A. V., Ariff, B. and Long, Q., Blood flow and vessel mechanics in a physiologically realistic model of a human carotid arterial bifurcation. *J. Biomech.*, 2000, **33**, 975–984.
17. Starmans-Kool, M. J., Stanton, A. V., Zhao, S., Xu, X. Y., Thom, S. A. M. and Hughes, A. D., Measurement of Hemodynamics in human carotid artery using ultrasound and computational fluid dynamics. *J. Appl. Physiol.*, 2002, **92**, 957–961.
18. Wake, A. K., *Modeling Fluid Mechanics in Individual Human Carotid Arteries*, Ph D thesis, Georgia Inst. Tech., 2005.
19. Allan, P. L., Dubbins, P. A., Pozniak, M. A. and McDicken, W. N., *Clinical Doppler ultrasound*, Churchill Livingstone, London, 2000.
20. Spencer, M. P. and Reid, J. M., Quantification of carotid stenosis with continuous-wave (C-W) Doppler ultrasound. *Stroke*, 1978, **10**, 326–330.
21. Kamouchi, M., Kishikawa, K., Okada, Y., Inoue, T., Ibayashi, S. and Iida, M., Reappraisal of flow velocity ratio in common carotid artery to predict Hemodynamic change in carotid stenosis. *Am. J. Neuroradiol.*, 2005, **26**, 957–962.
22. Nederkoom, P. L., Graaf, Y. V. and Hunink, M. G. M., Duplex ultrasound and magnetic resonance angiography compared with digital subtraction angiography in carotid artery stenosis: a systematic review. *Stroke*, 2003, **34**, 1324–1331.
23. Sabeti, S. *et al.*, Quantification of internal carotid artery stenosis with Duplex US: comparative analysis of different flow velocity criteria. *Radiology*, 2004, **232**, 431–439.
24. Sherwin, S. J. and Blackburn, H. M., Three-dimensional instabilities and transition of steady and pulsatile axisymmetric stenotic flow. *J. Fluid Mech.*, 2005, **533**, 297–327.
25. Verghese, S. S., Frankel, S. H. and Fischer, P., Direct numerical simulation of stenotic flows, part II: pulsatile flow. *J. Fluid Mech.*, 2007, **582**, 281–318.

ACKNOWLEDGEMENTS. We thank several staff members of MSRSAS and MSR Hospitals for their help. We appreciate the authorities of MSR Hospitals who have generously allowed us the use of equipment from the Department of Radiology. We also thank Directorate of Extramural Research and Intellectual Property Rights, DRDO for financial assistance.

Received 24 March 2009; revised accepted 4 September 2009